Transport in an idealized three-gyre system with application to the Adriatic Sea

I. I. Rypina,[1] L. J. Pratt,[1] M. G. Brown,[2] I. A. Udovydchenkov,[1] and H. Kocak[3]

[1]Woods Hole Oceanographic Institution, Woods Hole, MA, USA, [2]RSMAS, University of Miami, Miami, FL, USA,
[3]Department of Computer Science and Mathematics, University of Miami, Coral Gables, FL, USA,

What controls intergyre transport in a perturbed three-gyre system?

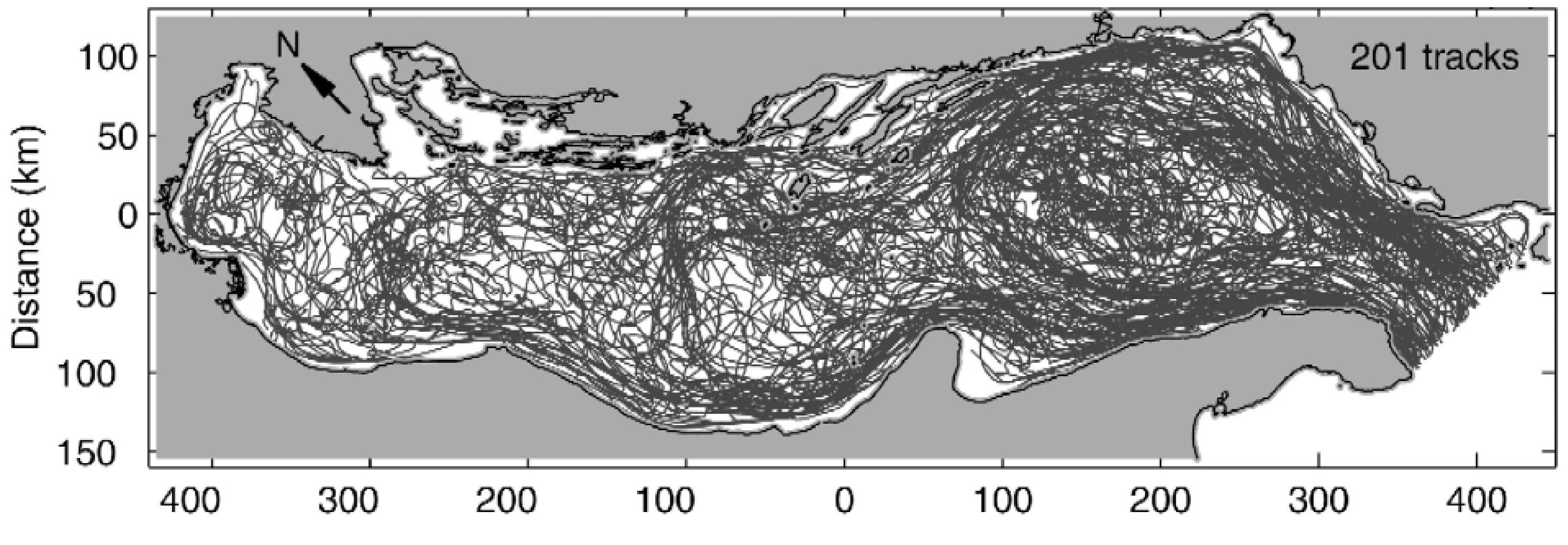

Figure 1. Tracks of 201 surface drifters in the Adriatic Sea between 1 August 1990 and 31 July 1999. (figure adapted from P.-M. Poulain, *J. Marine Systems*, **29**, 2001)

Introduction

Motivated by observations of surface drifters in the Adriatic Sea (see above), transport in a three-gyre system is studied with the aid of dynamical systems techniques. The velocity field is assumed to be two-dimensional and incompressible, and composed of a steady three-gyre background flow on which a time-dependent perturbation is superimposed. Two systems of this type are considered: 1) an analytical model of the Adriatic Sea; and 2) an observationally-based altimetry derived model of the Adriatic Sea. It is shown that a new phenomenon arises in a three-gyre system, which is not present in a two-gyre system. Due to this phenomenon, the three-gyre system has qualitatively different transport properties for small and large perturbations to the background. For a small perturbation two of the gyres exchange no fluid with the third gyre. When the perturbation strength exceeds a certain threshold, transport between all three gyres occurs[1].

Dynamical systems theory

• Lagrangian equations of motion

Assumptions of two-dimensionality and incompressibility allow one to introduce a streamfunction,

$$\psi(x,y,t),\ u=-\partial\psi/\partial y,\ v=\partial\psi/\partial x.$$

The Lagrangian equations of motion are then

$$\frac{dx}{dt}=-\frac{\partial\psi}{\partial y},\ \frac{dy}{dt}=\frac{\partial\psi}{\partial x}.$$

These equations have Hamiltonian form with the streamfunction playing the role of the Hamiltonian $\psi(x,y,t) \iff H(p,q,t)$. The streamfunction is assumed to consist of a steady background subject to a time-dependent perturbation

$$\psi(x,y,t)=\psi_0(x,y)+\psi_1(x,y,t).$$

• Action-angle variables (I,θ)

describe the unperturbed (steady) motion.

$$\psi_0(x,y)\rightarrow H(I)$$

$$\begin{cases} I=\frac{1}{2\pi}\oint x(y,H)\,dy=-\frac{1}{2\pi}\oint y(x,H)\,dx \\ \theta=\frac{\partial G}{\partial I} \text{ with } G(y,I)=\int_0^y x(y',H)\,dy' \end{cases}$$

$$\begin{cases} \dot I=-\frac{\partial H}{\partial \theta}=0 \\ \dot\theta=\frac{\partial H}{\partial I}\equiv\omega(I) \end{cases} \Longrightarrow \begin{cases} I(t)=const \\ \theta(t)=\omega(I)t+\theta_0 \end{cases}$$

I is an unperturbed trajectory label. Motion is periodic with period $2\pi/\omega(I)$. $\omega'(I)=d\omega/dI$ is a measure of shear. All trajectories are regular (nonchaotic) curves. No chaotic trajectories are present.

• Kolmogorov-Arnold-Moser (KAM) theorem

$$\psi(x,y,t)=\psi_0(x,y)+\varepsilon\psi_1(x,y,t)$$

1) quasiperiodic perturbation: $\psi_1(x,y,\sigma_1 t,...,\sigma_N t)$

2) Diophantine condition: $\{\sigma_i/\sigma_j,\omega/\sigma_i\}, i,j=1,...,N$ are sufficiently irrational

3) nondegeneracy condition (Russmann): $\omega(I)\neq const$

$\Longrightarrow$ surviving tori (barriers for transport)

• Strong KAM stability near shearless tori

$$\Delta\omega \propto \left(\varepsilon\left|\omega'\right|\right)^{1/2}$$

low values of shear

$\Longrightarrow$ small resonance widths

$\Longrightarrow$ resonances less likely to overlap

$\Longrightarrow$ surviving KAM tori

$\Longrightarrow$ barriers to transport

Two models of the Adriatic Sea

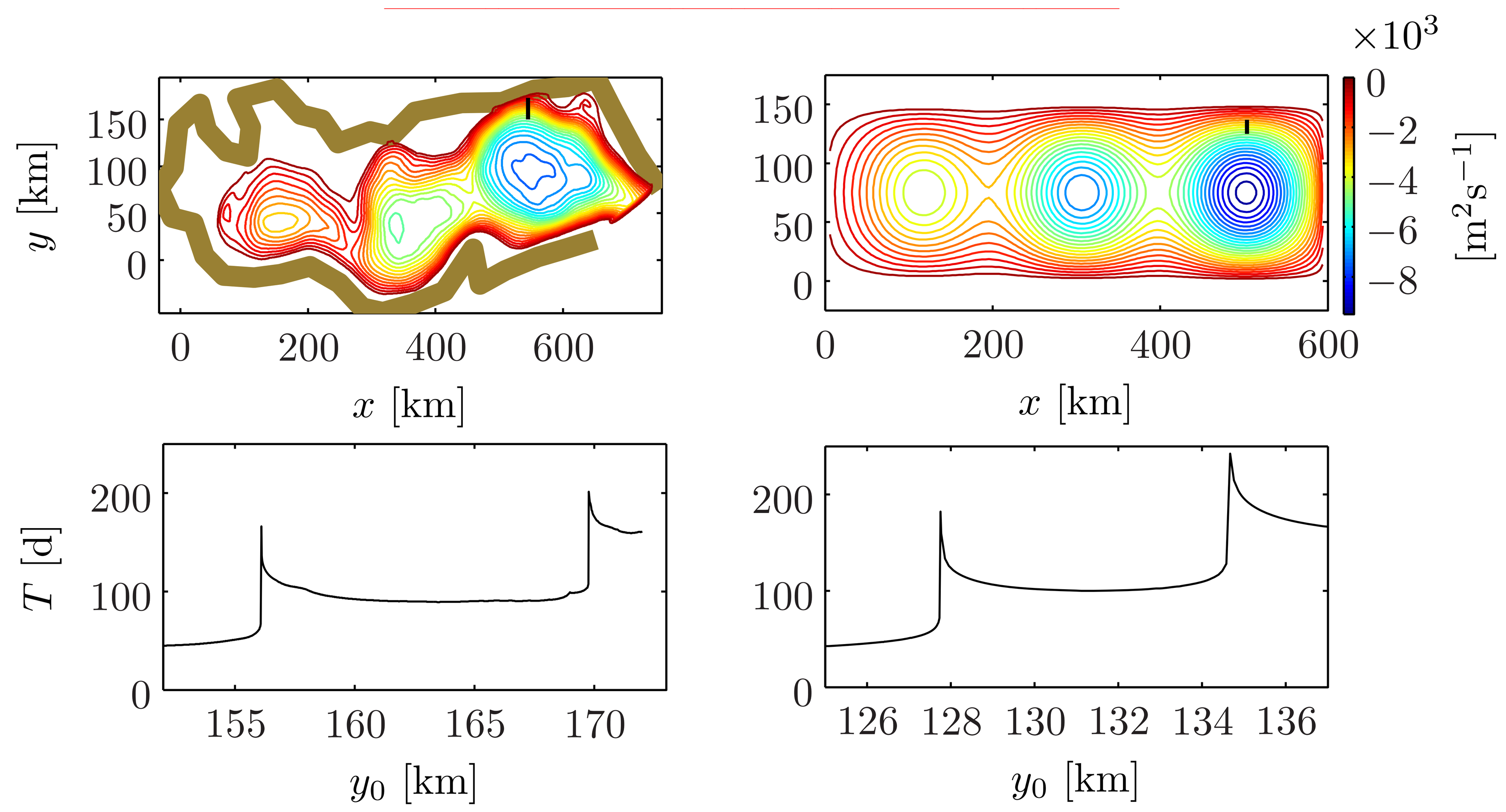

Figure 2. (Upper left) Level surfaces of the drifter-derived streamfunction, which describes the mean surface circulation in the Adriatic Sea. The thick brown line shows the smoothed boundary of the basin. Black dots at $x=545$ km show the initial positions of the trajectories that were used to produce the lower left plot. (Upper right) Level surfaces of the analytical streamfunction. Black dots at $x=500$ km show the initial positions of the trajectories that were used to produce the lower right plot. (Lower panels) Periods of simulated trajectories, T, for a family of trajectories with variable initial position, y_0.

3 gyre geometry. Shearless trajectory

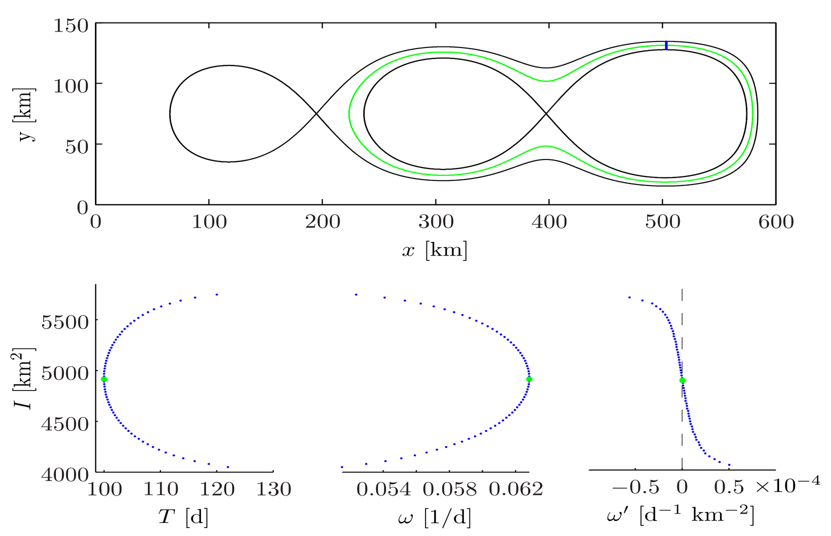

Figure 3. (Upper panel) For the three-gyre background steady flow, homoclinic orbits are shown in black, and the shearless trajectory is shown in green. (Lower panels) Plots of $T(I)$ (left), $\omega(I)$ (middle), and $\omega'(I)$ (right) for trajectories lying between the two homoclinic trajectories for the analytically described streamfunction. I is an unperturbed trajectory label. Motion is periodic with period $2\pi/\omega(I)$. $\omega'(I)$ is a measure of shear.

Schematic diagram

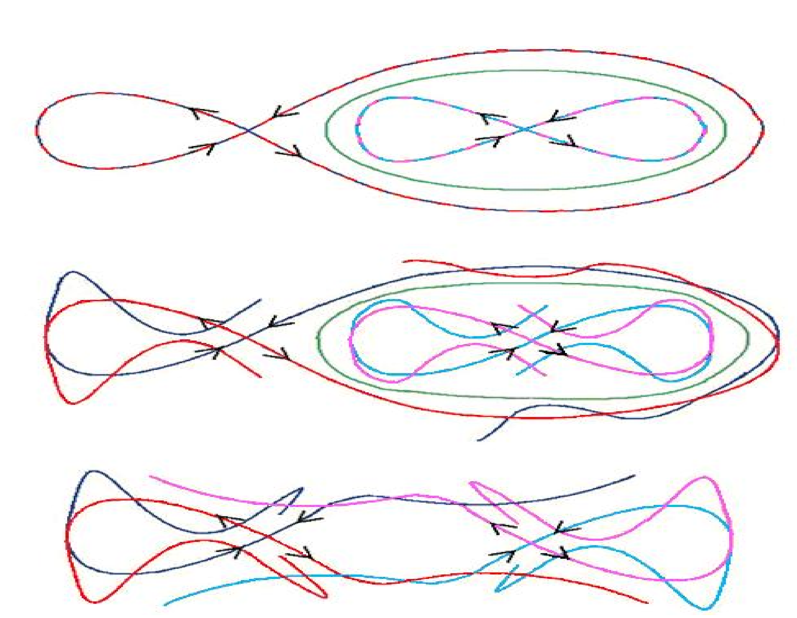

Figure 4. (Upper) The unperturbed system, $\varepsilon=0$. Homoclinic trajectories are shown as dashed red-blue curves. The shearless torus is shown in green. (Middle) Weak perturbation, $\varepsilon<\varepsilon_{cr}$. Stable/unstable manifolds are shown in blue/red. All manifold intersections are of the homoclinic type. A KAM invariant torus near the shearless trajectory is shown in green. This structure serves as a transport barrier that: 1) prevents heteroclinic manifold intersections from forming; and 2) isolates the western gyre from the central and eastern gyres. (Lower) Strong perturbation, $\varepsilon>\varepsilon_{cr}$. All KAM invariant tori near shearless trajectory are broken, thereby allowing heteroclinic manifold intersections to form, which, in turn, facilitate gyre-to-gyre-to-gyre transport.

Simulations in the analytical model

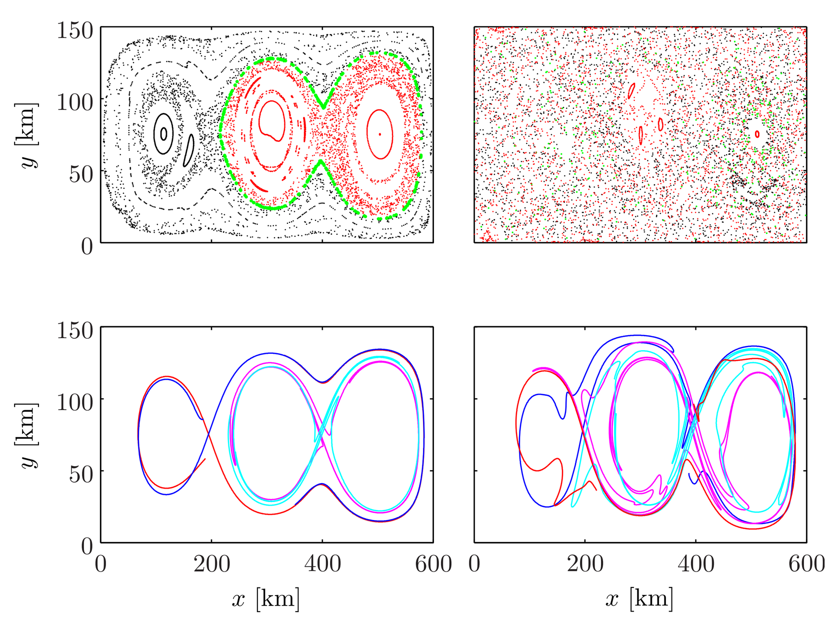

Figure 5. Simulations for two values of ε: $\varepsilon=0.05$ on the left and $\varepsilon=0.3$ on the right. (Upper plots) Poincare sections for an analytically steady streamfunction subject to a periodic perturbation. A KAM invariant torus is shown in green on the upper left subplot. Note that it serves as a transport barrier for the color-coded trajectories whose initial positions are inside (red dots) and outside (black dots) the close curve. (Lower plots) Stable (blue and light blue curves) and unstable (red and pink curves) manifolds of hyperbolic trajectories for an analytical steady streamfunction subject to a quasiperiodic perturbation.

Observationally-based model: $\psi=\psi_{drifter-based}+\epsilon\psi_{altim}$

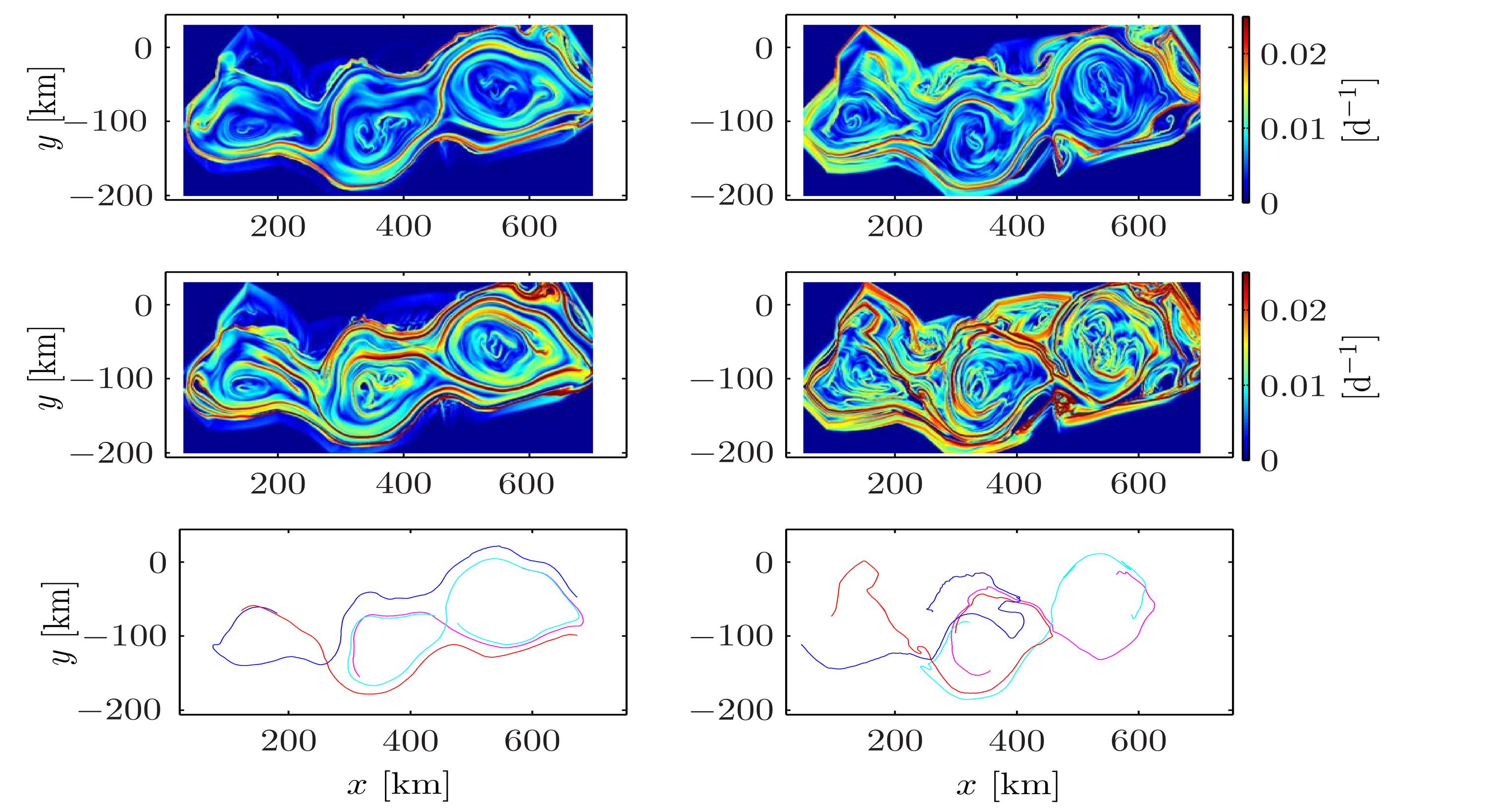

Figure 6. Simulated stable/unstable manifolds in the observationally-based model for two values of ε: $\varepsilon=0.1$ on the left; and $\varepsilon=1$ on the right. (Upper) FTLE estimates computed in forward time relative to $t=182$ days. Ridges of intense red correspond to stable manifolds. (Middle) FTLE estimates computed in backward time relative to $t=182$ days. Ridges of intense red correspond to unstable manifolds. (Lower) Stable and unstable manifolds computed using the direct manifold integration method relative to $t=182$ days. Note that on the left all manifold intersections are of the homoclinic type, while on the right both homoclinic and heteroclinic intersections of manifolds are present.

Lobe dynamics

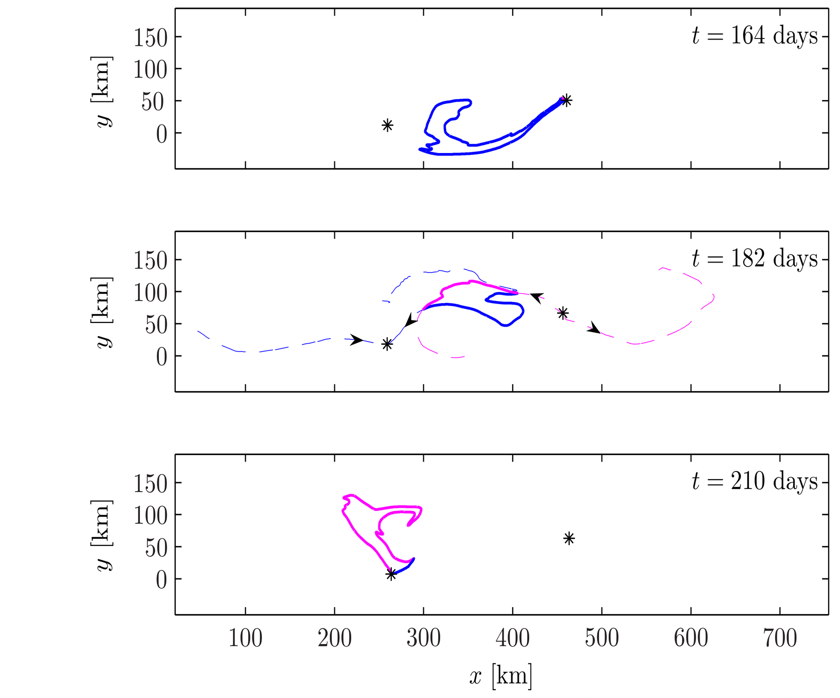

Figure 7. Simulations of the evolution of a heteroclinic lobe in forward and backward time relative to $t=182$ days using the observationally-based model with the true value of the perturbation strength, $\varepsilon=1$. The boundary of the heteroclinic lobe is shown at the times indicated in the three panels. The portion of the boundary of the lobe that is comprised of a segment of the unstable manifold is shown in pink; the portion of the boundary of the lobe that is comprised of a segment of the stable manifold is shown in blue. Positions of the two hyperbolic trajectories are shown with asterisks. In the middle subplot, the stable and unstable manifolds which form the heteroclinic lobe are shown by dashed blue and dashed pink lines. Arrows on the manifolds indicate the direction of attraction/repulsion.

Transport for small and large perturbation

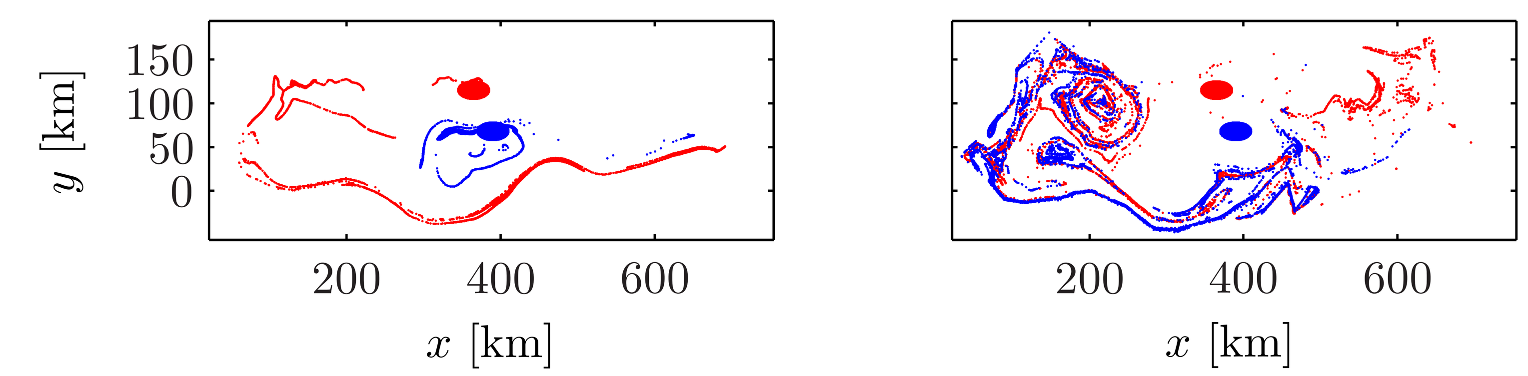

Figure 8. Initial ($t=182$ days) and final ($t=302$ days) positions of two sets of passive tracers in the observationally-based model for two values of the perturbation: $\varepsilon=0.1$ (left) and $\varepsilon=1$ (right). The two sets of tracers are color-coded. The initial positions of the two sets of tracers lie inside two circles. Note that for $\varepsilon=0.1$ there is no mixing (in a coarse-grained sense) of red and blue tracers, while for $\varepsilon=1$ there is strong mixing.

Conclusions

- Transport is qualitatively different for small and large perturbation to the background.
- For a small perturbation: 1) a transport barrier of the strong KAM stability type isolates the central and eastern gyres from the western gyre; and 2) all manifold intersections are of the homoclinic type
- For a large perturbation: 1) the transport barrier is broken; and 2) both homoclinic and heteroclinic intersections of manifolds are present. It is the presence of heteroclinic intersections of manifolds that makes gyre-to-gyre-to-gyre transport possible.

Acknowledgements. Work supported by NSF, grants CMG0417425 and CMG82469600.

References

1. I. I. Rypina, M. G. Brown, and H. Kocak. Transport in an idealized three-gyre system with an application to the Adriatic Sea. *J. Phys. Oceanogr.*, 39(3):675–690, 2009.